Biosensors and Bioelectronics 170 (2020) 112636

Contents lists available at ScienceDirect

Biosensors and Bioelectronics

journal homepage: http://www.elsevier.com/locate/bios

Smart plant-wearable biosensor for in-situ pesticide analysis

Fengnian Zhao [a], Jianwei He [b], Xunjia Li [a], Yunpeng Bai [b,*], Yibin Ying [a,c], Jianfeng Ping [a,**]

[a] Laboratory of Agricultural Information Intelligent Sensing, School of Biosystems Engineering and Food Science, Zhejiang University, 866 Yuhangtang Road, Hangzhou, 310058, PR China
[b] State Key Laboratory of Bioreactor Engineering, East China University of Science and Technology, 130 Meilong Road, Shanghai, 200237, PR China
[c] Zhejiang A&F University, Hangzhou, 311300, PR China

ARTICLE INFO

Keywords:
Wearable biosensor
Graphene
In-situ analysis
Pesticide residue
Precision agriculture

ABSTRACT

Inspired by the wearable sensors and to meet the demand for rapid and nondestructive detection, we developed a smart plant-wearable biosensor, which can be applied for in-situ analysis of organophosphorus pesticide on crop surfaces. Herein, the serpentine three-electrode system was prepared via the laser-induced graphene (LIG) technology. After transferred by polydimethylsiloxane (PDMS), the stretchable and flexible LIG-based electrode was obtained, which can be well adapt to the irregular surface of crops, such as leaves and fruits. After modified with organophosphorus hydrolase (OPH) and equipped with biocompatible semisolid electrolyte, our plant-wearable biosensor can selectively capture and recognize the methyl parathion and the data can be transmitted to a smartphone device wirelessly, which enable the real-time and in-situ electrochemical analysis of pesticide on the surface of agricultural products. To further enhance the electrochemical performance, gold nanoparticles (AuNPs) were modified on the surface of three-dimensional (3D) porous LIG. Such smart plant-wearable biosensor could be a transformative approach for the in-situ analysis of pesticide residue on crops, which could also promote the development of precision agriculture in the future.

1. Introduction

Recent years, remarkable progress have been achieved for stretchable and flexible electronics with the development of material science, which have gradually improved living quality for human beings (Mishra et al., 2017; Xuan et al., 2018). Among them, wearable biosensor, which can directly attach on the wearer's body, is a star attraction due to the continuous, noninvasive, and real-time properties during the dynamic analysis process (Kim et al., 2019). However, most of wearable biosensors have only been applied for fitness and healthcare monitoring for human beings, such as ions (e.g. Na^{+}, Ca^{2+}, and pH) (Guinovart et al., 2014; Nyein et al., 2016) and molecules (e.g. lactate, glucose, and alcohol) (Ashley et al., 2019; Xuan et al., 2018) in biofluids, as well as physiological signals (e.g. temperature, humidity, and electrocardiogram) (Imani et al., 2016; Ma et al., 2018). Aimed at the global demand for food, some researchers have turned their attention to plant sensors to enable sustainable agricultural production (Giraldo et al., 2019; Li et al., 2019).

Plant sensor is a promising device in agricultural production, which can collect the real-time information of plant physiological status (Giraldo et al., 2019). Not only has this feature, plant-wearable sensor can be easily attached on soft plant surfaces owning to the excellent mechanical compatibility (Lan et al., 2020). The collection of real-time information via plant-wearable sensor make the fine-tuning of resource inputs before symptoms possible, which is of significance for the development of agricultural sustainability (Hofmann et al., 2020). Up to now, plant-wearable sensor has been explored for the monitoring of plant growth (Nassar et al., 2018; Tang et al., 2017, 2019), relative humidity (RH) (Lee et al., 2014), and plant diseases (Li et al., 2019; Paul et al., 2019). The assessment of these indicators could offer the real-time information about the plant health and specific needs. Except for that, the assessment and sensing of agrochemicals, like pesticides, also plays essential part for the development precision agriculture (Zhao et al., 2020). However, in order to improve the crop yield, the cases of abuse and improper use of pesticides emerge frequently, which could cause the problem of pesticide residue, further inducing serious threat for human beings (Cui et al., 2018; Zhao et al., 2018a). Recently, even though many analytical technologies have been developed for pesticide detection, the complicated sample pretreatment is still essential in real sample analysis (Zhao et al., 2018b, 2019), which could not meet the demand for rapid

* Corresponding author.,
** Corresponding author.
E-mail addresses: ybai@ecust.edu.cn (Y. Bai), jfping@zju.edu.cn (J. Ping).

https://doi.org/10.1016/j.bios.2020.112636
Received 27 June 2020; Received in revised form 2 September 2020; Accepted 17 September 2020
Available online 18 September 2020

and nondestructive analysis. To address this challenge, in-situ detection of pesticide, such as surface-enhanced Raman scattering (SERS) on crop surface comes into being (Chen et al., 2020; Nguyen Thi et al., 2020; Sitjar et al., 2019). However, few researches focus on electrochemical technology for in-situ pesticide analysis on crop surfaces (Mishra et al., 2017).

In this work, we proposed a plant-wearable electrochemical biosensor, which can be attached on the crop surface for in-situ analysis of organophosphorus pesticide (OP) (Fig. 1). Herein, the 3D porous laser-induced graphene (LIG)-based serpentine three-electrode was fabricated by direct writing on commercial polyimide (PI) film using the computer-controlled laser induction system (Ye et al., 2019; You et al., 2019). After transferred by polydimethylsiloxane (PDMS), the flexible and stretchable plant-wearable sensor was obtained, which can be well adapt to the irregular crop surfaces and the potential deformation caused by the environmental factors. After modified with organophosphorus hydrolase (OPH) and equipped with biocompatible semisolid electrolyte, our plant-wearable biosensor can selectively capture and recognize the methyl parathion on crop surfaces. By virtue of a hand-held electrochemical workstation equipped with Bluetooth, the real-time information of pesticide residue can be received wirelessly on a smartphone. This plant-wearable analytical strategy dispenses with the complicated sample pretreatment, which could meet the rapid, nondestructive, and in-situ recognition of pesticide on crop surfaces.

2. Experimental

2.1. Materials

The commercial PI film (25 μm, Dupont TM, USA), Ag/AgCl ink (E2414, Ercon, Inc., MA), and PDMS (Dow Corning Co, USA) were used in this study. Gold (III) chloride trihydrate ($HAuCl_4{\cdot}3H_2O$), Nafion, methanol, and ethanol were bought from Sigma Aldrich (St. Louis, MO, USA). Methyl parathion, dipotassium hydrogen phosphate (K_2HPO_4), potassium dihydrogen phosphate (KH_2PO_4), and gelatin were obtained from Aladdin Bio-Chem (Shanghai, China). In this study, the employed OPH enzyme was methyl parathion hydrolase, which was obtained from *E. coli BL21* (DE3) fermentation (Luo et al., 2014).

2.2. Instruments

3D porous LIG was prepared on the PI film using a computer-controlled laser scribing micromachine (Nano Pro-III, Tianjin Jiayin Nanotechnology Co., Ltd., China). Electrochemical experiments were performed with a hand-held electrochemical workstation (EmStat3 Blue, PalmSens, Netherlands), for which the data can be transmitted to a smartphone equipped with the APP through Bluetooth. The mechanical study was achieved by a tensile testing instrument (UTM2203, Sun Technology Stock Co., Ltd). The morphology and chemical composition of the LIG were characterized by a field emission scanning electron microscope (HITACHI-SU8010, Japan) and a LabRAM HR Evolution Raman microscope system (Horiba Jobin Yvon, Kyoto), respectively.

2.3. Fabrication of flexible LIG-based electrode

The flexible three-electrode system (PDMS/LIG) was prepared flowing the following steps (Fig. 1). Before the operation, the commercial polyimide (PI) sheet was placed on a glass and then stuck by the polymeric methyl methacrylate (PMMA) mold. Then, the PI sheet was patterned using the computer-controlled laser system to obtain the 3D porous LIG. Next, the patterned PI film was covered with liquid PDMS and then heated at 75 °C for 120 min. After that, the side of PDMS/LIG was peeled off from the PI film to obtain the flexible and stretchable LIG-based electrode. The serpentine conductive areas in the middle were insulated by coating with liquid PDMS and same thermal treatment. Finally, the Ag/AgCl ink was coated on the exposed reference electrode and heated until curing.

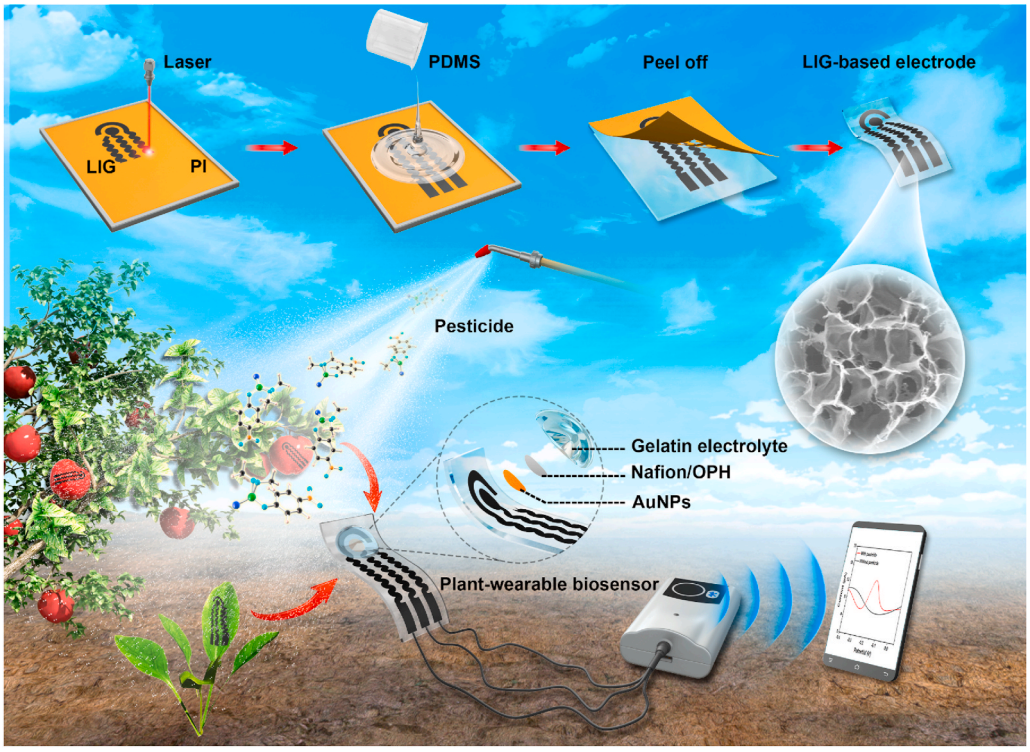

Fig. 1. Schematic diagram of the fabrication process of the plant-wearable biosensor based on 3D porous LIG and the application of in-situ pesticide analysis for agricultural products.

2.4. Preparation of plant-wearable biosensor

Herein, Nafion was used to promote the immobilization of OPH enzyme. First of all, the OPH solution in 0.1 M phosphate buffer solution (PBS) (pH = 6) and 0.2% Nafion in ethanol were prepared, severally. Then, the OPH and Nafion solutions were mixed with a volume ratio of 1:1, and 10 μL of the mixture was drop-casted onto the sensing area of the PDMS/LIG electrode. After dried at room temperature, the functionalized biosensor was fabricated. To enhance the sensing behavior, the PDMS/LIG electrode was decorated with Au nanoparticles (AuNPs) with the method of electrochemical deposition in 1% $HAuCl_4$ solution for 60 s. After modified with the same bio-reagent layer (Nafion/OPH), the plant-wearable biosensor (LIG-Au-OPH) was prepared.

2.5. Electrochemical measurement

The hand-held electrochemical workstation was applied for the measurement of electrochemical behaviors. To explore the preparation condition of the LIG-based electrode and the effect of applied strain on electrochemical behavior, the cyclic voltammetry (CV) measurement was performed in 0.1 M KCl solution containing 1.0 mM K_3 $[Fe(CN)_6]$ over the voltage range between −0.3 V and +0.5 V with a scan rate of 0.05 V s^{-1}. The OP sensing was carried out from −0.6 V to +0.4 V in the PBS solution (0.1 M, pH = 6) using square wave voltammetry (SWV) with the frequency of 8 Hz and equilibration time of 30 s.

2.6. In-situ pesticide analysis on crop surfaces

The leaf of spinach and the fruit of apple were regarded as the target crop surfaces. Before the test, the crop surfaces were washed with distilled water and thoroughly dried. After that, methyl parathion solution (100 μM) was sprayed on the target surfaces and totally dried at room temperature. The gelatin semisolid electrolyte was adopted between the solid surfaces. Briefly, 2.5 wt % gelatin was added in a 100 mM KCl and 100 mM KH_2PO_4 buffer and then heated until completely dissolving. After adjusting the pH to 6, the above mixture was aged overnight to form gel at room temperature. Finally, the gelatin electrolyte (0.5 ± 0.03 mm of thickness) was coated on sensing area. The in-situ pesticide analysis was achieved using SWV with the frequency of 8 Hz and equilibration time of 30 s after pasting the biosensor equipped with semisolid electrolyte on target surface.

3. Results and discussion

3.1. Characterization of LIG-based electrode

Laser power and scan speed are the main factors for the morphology and electrochemical property of porous LIG. From Figs. S1a–c and Fig. 2a, the higher power, the more porous graphene comes into being. Comparing the CV responses of the PDMS/LIG electrodes (Fig. 2b), the increase of 3D porous structure under higher power contributes to the increase of conductivity. However, the glass under PI sheet would also be patterned after sequentially increasing the power. Consequently, we chose 3.6 W as the optimized power. As for the influence of scan speed (Figs. S1d–e), more multilayer graphene walls will form on the porous structure at slower scan speed (Lamberti et al., 2016; Zhang et al., 2020). When the scan speed is too slow (Fig. S1f), the collapse of 3D porous structure appears, indicating the destruction of the graphene structure. The corresponding CV responses (Fig. 2c) also verify that the electrochemical activity would be affected by the collapse. Thus, 20 cm s^{-1} was set as the optimized speed.

Raman spectrum was applied to verify the presence of graphene in the prepared material. From Fig. 2d, the optimized porous materials have three prominent Raman peaks, including D band (~1350 cm^{-1}), G

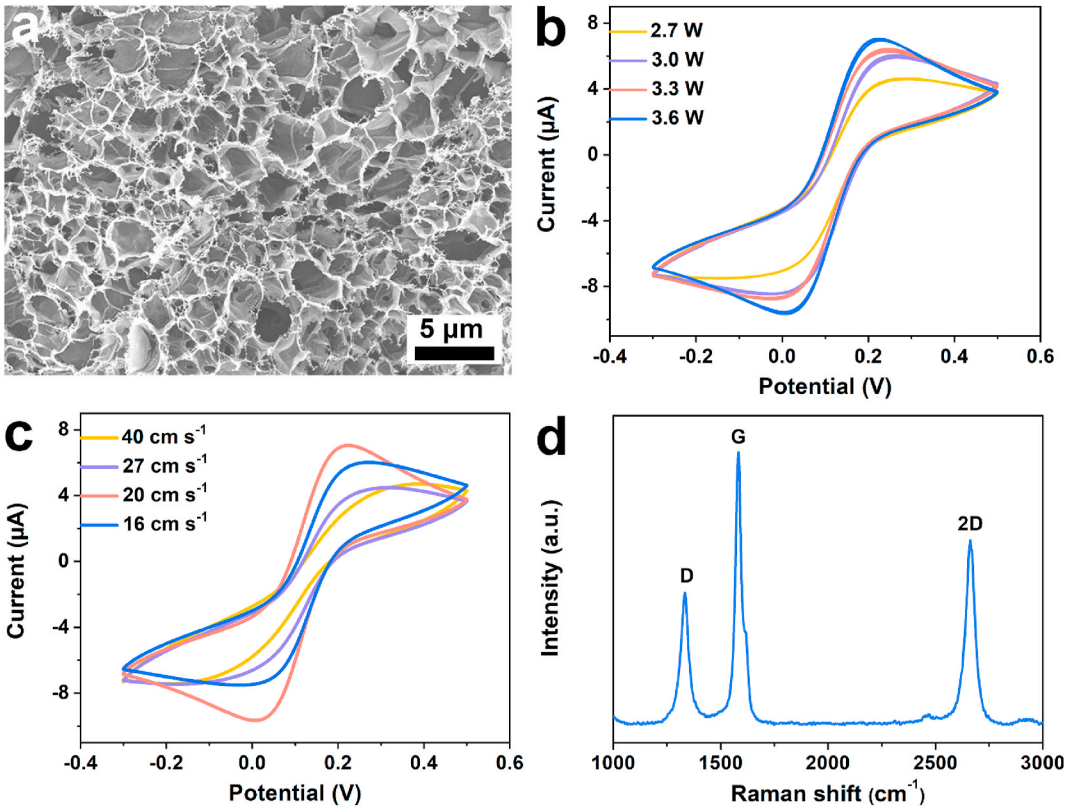

Fig. 2. Characterization of the obtained flexible LIG-based electrode. (a) SEM image of the porous LIG (3.6 W and 20 cm s^{-1}). CV response of the electrode with different (b) power and (c) scan speed in 0.1 M KCl solution containing 1.0 mM K_3 $[Fe(CN)_6]$. (d) Raman spectrum of the porous LIG under the optimized condition (3.6 W and 20 cm s^{-1}).

band (~1580 cm^{-1}), as well as 2D band (~2700 cm^{-1}). While 2D band and G band are exactly corresponding to the typical peaks for graphene materials (Chyan et al., 2018; Lin et al., 2014). Combined with SEM images, our prepared porous LIG indeed has the intrinsic property of graphene.

3.2. Study of mechanical deformation

In this study, the prepared PDMS/LIG electrode is flexible and transparency, which is allowed for twisting (Fig. 3a). To adapt to the irregular crop surfaces and the potential deformation caused by the environmental factors like wind, the satisfying mechanical properties are necessary for plant-wearable sensor. Therefore, we studied the effect of different mechanical deformations on the flexible electrode. Firstly, we investigated the resistance change when our electrode was subjected to stretching. As showed in Fig. 3b, our serpentine electrode appears acceptable variation of resistance, which can stand for the applied strain of over 10%. Even though the tensile strength is not very remarkable compared with the reported wearable sensors, it is enough to adapt to the possible shape change for most of vegetables and fruits in the short term. The electrochemical performance of the flexible electrode during the process of stretching was evaluated using CV measurement. Fig. 3c displays the CV curves with and without the applying of 5% stretching. It is clear that, the 5% stretching only caused a negligible change for the CV response compared with the original one, indicating the promising tensile strength of the obtained flexible electrode.

After that, we explored the electrochemical behavior of the electrode on the simulative agricultural product surface. Specifically, the LIG-based electrode was placed along with the curved surface of culture dishes of different diameters (3.5, 5.5, and 9 cm) to get various bending angles (~25, 16, and 10°), and explored its electrochemical response during the bending process. As shown in Fig. 3d, the bending process can cause insignificant influence upon the CV response, further verifying our electrode can adapt to the curved surfaces, making the in-situ detection on the surface of vegetables and fruits possible. We also investigated the mechanical deformation of the electrode after modification with AuNPs (PDMS/LIG-Au). It is clear that the PDMS/LIG-Au electrode can also keep the similar electrochemical response during the process of stretching and bending (Fig. S2).

3.3. Pesticide sensing

To further enhance the electrochemical performance, AuNPs were decorated by the electrochemical deposition with a constant potential of −0.66 V for 60 s. As seen in SEM and EDS images (Fig. 4b and Figs. S3e–h), the AuNPs have been decorated over the porous surface of PDMS/LIG electrode (Fig. 4a and Figs. S3a–d), which could offer larger electroactive surface area. From Fig. 4c, the CV response of PDMS/LIG-Au electrode (yellow line) is higher than that of PDMS/LIG electrode (blue line), indicating its excellent properties of electron transfer and conductivity.

As the selective bio-recognition element, OPH can hydrolyze methyl parathion to release the electroactive *p*-nitrophenol (PNP) (Ye et al., 2016). Before the sensing of methyl parathion, we compared the catalytic activity of PDMS/LIG-Au and PDMS/LIG electrode in PNP solution (0.1 M PBS, pH = 7) by the SWV measurement. As illustrated in Fig. 4d, the well-defined peak appears around −0.10 V for PDMS/LIG-Au electrode, whose intensity is positively correlated with the concentration of PNP. Interestingly, not only the potential (~−0.10 V) of PDMS/LIG-Au electrode for PNP catalysis is lower than that of LIG electrode (~+0.85 V), the current signal is also higher in the same solution, indicating the AuNPs could accelerate the redox reaction on electrode surface. Hence, the PDMS/LIG-Au electrode was applied as the working electrode.

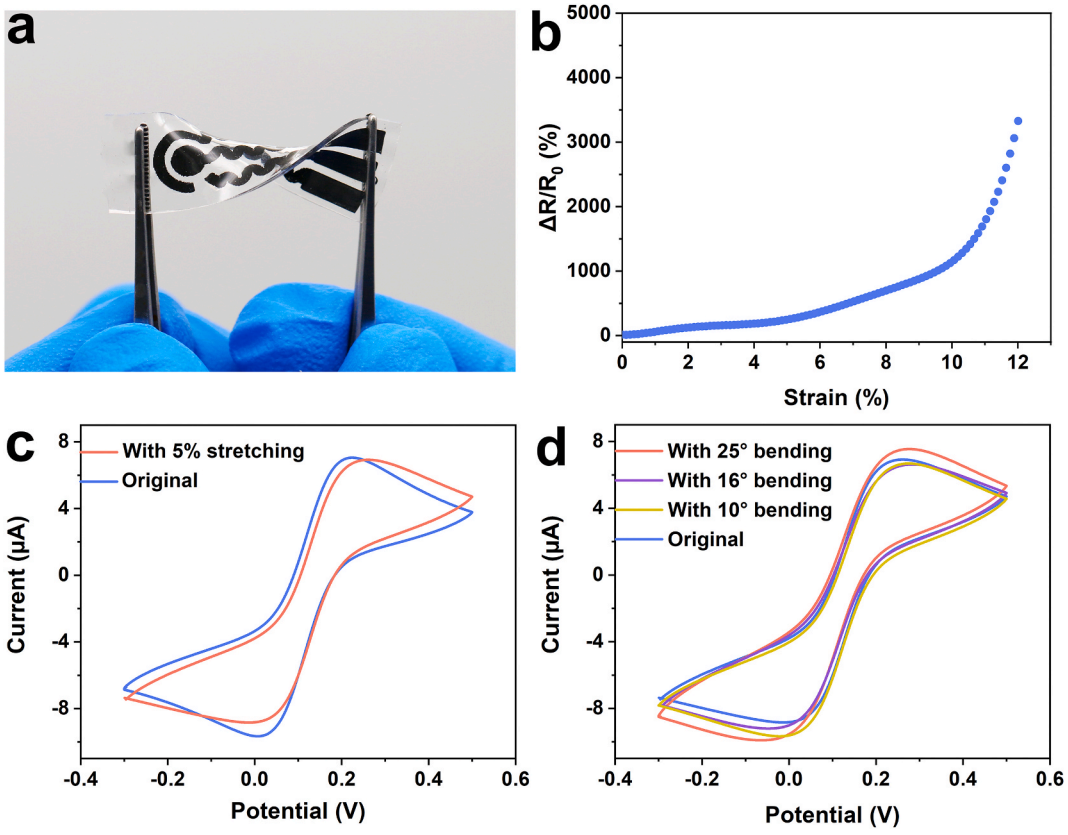

Fig. 3. Effect of applied strain for the fabricated PDMS/LIG electrode. (a) Digital photo of the electrode under twisting. (b) Resistance-strain curve of the electrode with the stretching. (c–d) CV curves of the electrode during the process of stretching (c) and bending (d) in 0.1 M KCl solution containing 1.0 mM K_3 $[Fe(CN)_6]$.

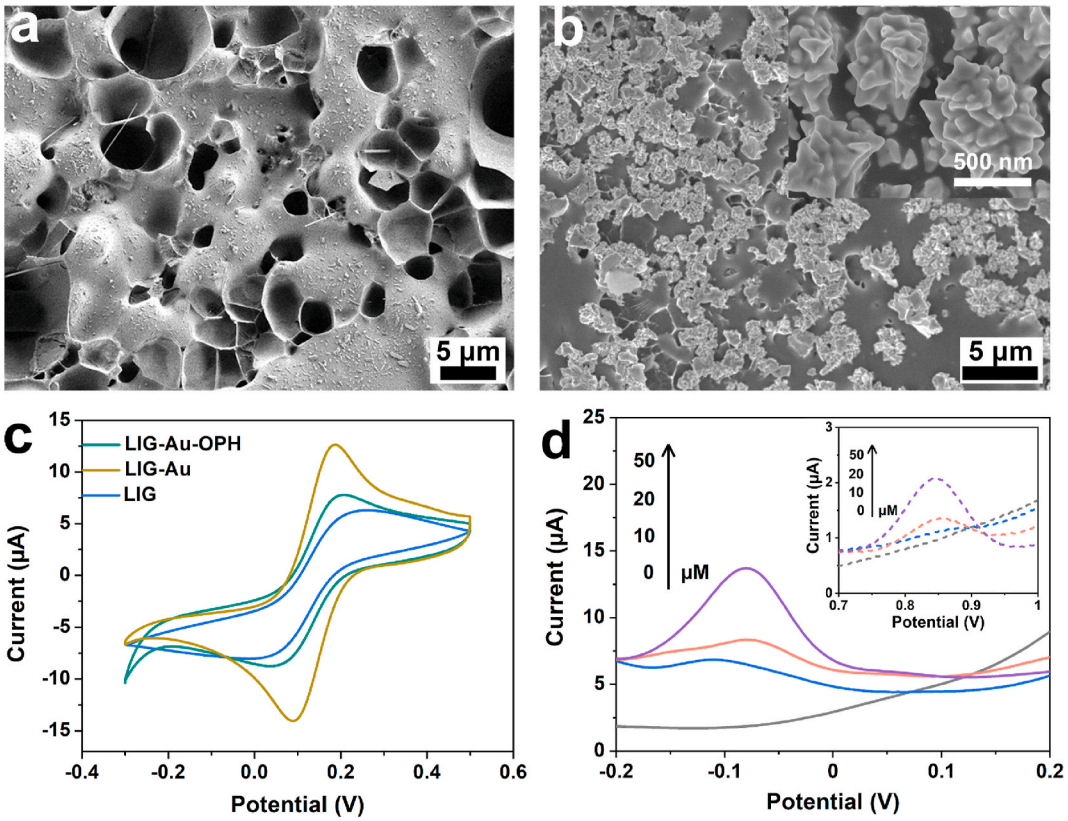

Fig. 4. Performance evaluation of the LIG-based electrode. (a–b) SEM images of the PDMS/LIG electrode before and after the modification of AuNPs. Insert in (b) is the magnification SEM image after the modification of AuNPs. (c) CV response of the various LIG-based electrodes in 0.1 M KCl solution containing 1.0 mM K_3 [Fe $(CN)_6$]. (d) The catalytic behavior of the PDMS/LIG-Au electrode for PNP. Insert is the catalytic behavior of the PDMS/LIG electrode for PNP.

Then, with the contribution of Nafion, the OPH enzyme was modified on the surface of electrode to obtain the LIG-Au-OPH biosensor (green line in Fig. 4c). It is clear that the CV response of LIG-Au-OPH biosensor gets lower compared with that of LIG-Au electrode, indicating the successful modification of OPH enzyme. To obtain the optimized sensing performance, the loading of OPH enzyme, the concentration of Nafion, and the pH of PBS solution were optimized by the comparison of SWV response in the addition of methyl parathion (100 μM) with the reaction time of 5 min. As presented in Fig. S4a, the current response gets to the maximum when the loading of OPH is 0.01 U. Continuing to increase the enzyme loading, the current response declines, indicating over-loaded OPH would block the electron transfer. Hence, the optimized OPH loading was set as 0.01 U. Nafion is the widely used electrode modifier to efficiently immobilize various enzymes on electrode surface avoiding leaching out during the detection process (Karyakin et al., 1996; Mishra et al., 2017; Patel et al., 2000). It has been reported that the enzyme-Nafion film from water-organic solutions with high concentration of organic solvent appears better sensitivity and stability (Karyakin et al., 1996). Therefore, Nafion (in ethanol) and OPH (in PBS solution) were mixed with a volume ratio of 1:1 in this study. However, the active sites of OPH may be obstructed by the excessive Nafion (Fig. S4b). Therefore, the optimized concentration for Nafion was 0.2%. Finally, the effect of different pH of PBS solution was investigated. It is clear that the SWV signal is higher when the pH of PBS solution below 7, that is probable due to the H^+ plays important part for the catalysis of PNP in this sensing system (Guo et al., 2015). Considering too low pH may cause influence for OPH activity, we chose 6 as the optimized pH value for electrolyte (Fig. S4c).

Different from the traditional mass transfer at the solid/liquid interface, the mass transfer between plant-wearable biosensor and crop surfaces is solid/solid interface. Hence, it's a challenge to realize the mass transfer of pesticide at this specific interface. Inspired by the group of Wang (Mishra et al., 2017), we adopted the gelatin semisolid electrolyte instead of the traditional liquid electrolyte. To evaluate the in-situ detection performance, the intact "electrochemical cell" (plant--wearable biosensor equipped with gelatin electrolyte) was attached on a piece of polyethylene terephthalate (PET) film, where methyl parathion solution (50 μM) was sprayed and dried at room temperature. Firstly, we optimized the reaction time of the biosensor equipped with semisolid electrolyte. Based on the original and base-line corrected SWV response (Fig. 5a–b), we finally chose 8 min as the optimized reaction time. It should be noticed that the *p*-nitrophenol peak shifts from −0.10 V (Fig. 4d) to −0.05 V. This is because the influence of the enzyme loading and the usage of semisolid electrolyte.

Under the optimized conditions, we investigated the corresponding relationship between the pesticide concentration and current signal by placing the biosensor on a series of PET films sprayed with different concentrations of methyl parathion. Fig. S5 displays the electrochemical response through SWV measurement. To make the measurement of peaks heights easily, we adopted the Origin software to obtain the corresponding baseline-corrected curves (Fig. 5c), which is of efficiency when peaks show as shoulders on steep flanks (Diego et al., 2010; Zhang et al., 2020). When the concentration of methyl parathion ranges from 20 μM to 500 μM, the corresponding current signal has a linear relation with the logarithm of its concentration. From the fitting curve (Fig. 5d), the linear equation is $I = 2.13\lg C - 2.69$ ($R^2 = 0.984$), where I stands for the corresponding current and C stands for the pesticide concentration. According to the equation of detection limit (LOD) = 3Sb/m (Sb represents the standard deviation of the SWV in the pesticide blank and m represents the slope of the calibration curve), the LOD of this biosensor for in-situ analysis of methyl parathion is 0.01 μM (i.e., 2.63 μg L^{-1}), which can meet the demand for the detection of methyl parathion in vegetables and fruits announced by the European Commission.

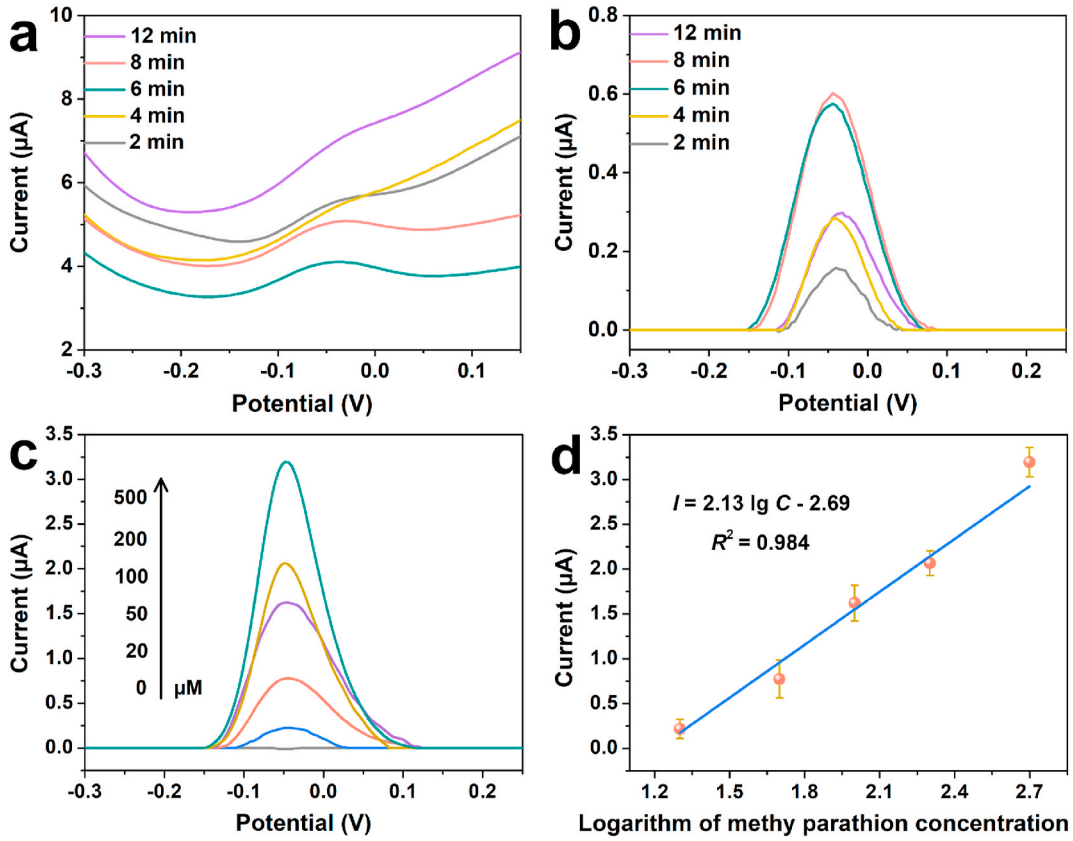

Fig. 5. Pesticide sensing of the plant-wearable biosensor on PET film. SWV response of (a) raw data curves and (b) baseline-corrected curves of the optimization of reaction time of the biosensor equipped with gelatin electrolyte. (c) Baseline-corrected SWV curves of the biosensor after placed on PET film contaminated with methyl parathion (0–500 μM). (d) The corresponding calibration curve.

3.4. In-situ analysis of real samples

Researches have revealed that non-systemic pesticides after spraying will mainly stay on the surface of crops until degradation (Chung, 2018). Consequently, it is of great instructive significance to get the residue information timely on crop surfaces. Herein, we chose spinach and apple as the typical agricultural products, where the methyl parathion solution (100 μM) was sprayed on the leaf of spinach and fruit of apple, respectively. After totally dried at room temperature, the flexible biosensor equipped with semisolid electrolyte was pasted on the surface of leaf or fruit due to its internal stickiness. Meanwhile, the control experiments without pesticide were carried out under the same condition. In our study, the employed OPH enzyme is thermostable (Luo et al., 2014), which can keep favorable activity on crop surfaces in natural environment. As presented in Fig. 6a and d, the sensing and test system can be connected successfully with the help of conductive silver tape. Through a smartphone equipped with the APP, the pesticide residue information on the surface of real samples can be obtained timely (Fig. 6b and **e**). Compared with the control experiments, the obvious *p*-nitrophenol peaks are observed in the samples in the presence of methyl parathion, which can realize the qualitative alert for the presence of pesticide at a particular moment. To make it clear, we also compared the curves after the baseline-corrected process (Fig. 6c and **f**). Compared with the SWV responses on PET film (Fig. 5c), the peak currents for leaf of spinach and apple are both lower. That is because the surfaces of agricultural products are more complicated. Even though the non-systemic pesticides (e.g. methyl parathion) after spraying will mainly stay on the surface of crops until degradation, limited penetration into the cuticle still occurs (Chung, 2018). Therefore, it is possible that the peak currents for leaf of spinach and fruit of apple are both lower than the response on PET film. In addition, these two different crop surfaces also appear the signal difference. That is because the pesticide penetration is harder owning to the protection of waxy skinned fruits. While the abundant stomas on leaf surface would benefit for the penetration (Lin et al., 2016). Calculated by the linear equation in Fig. 5d, we can still roughly estimate the residue level of pesticide, which will be conducive to understand the pesticide degradation process and judge the credible picking period for agricultural products.

4. Conclusions

In this work, we developed a smart plant-wearable biosensor for the in-situ detection of methyl parathion on the surface of crops. The favorable three-electrode system can be easily patterned using the LIG technology on the commercial PI film by controlling the laser power and scan speed. After transferred by PDMS, the stretchable and flexible LIG-based electrode can be prepared, which can still keep the satisfying electrochemical response during the process of stretching and bending. This smart plant-wearable biosensor modified with OPH and equipped with gelatin electrolyte can be attached on the surface of agricultural products, such as leave of spinach and fruits of apple, which allows for the real-time and in-situ analysis of methyl parathion by the electrochemical determination of the corresponding hydrolysis product. This work provides a novel approach for the acquisition of pesticide residue information, which gives new insight into the design of next generation wearable biosensor for future agriculture. Future efforts will focus on investigating the influence of environmental conditions (e.g. temperature and humidity) and various plant interfaces on plant-wearable biosensor. Moreover, the more stable recognition elements will be explored to satisfy the long-time monitoring during the whole plant growth.

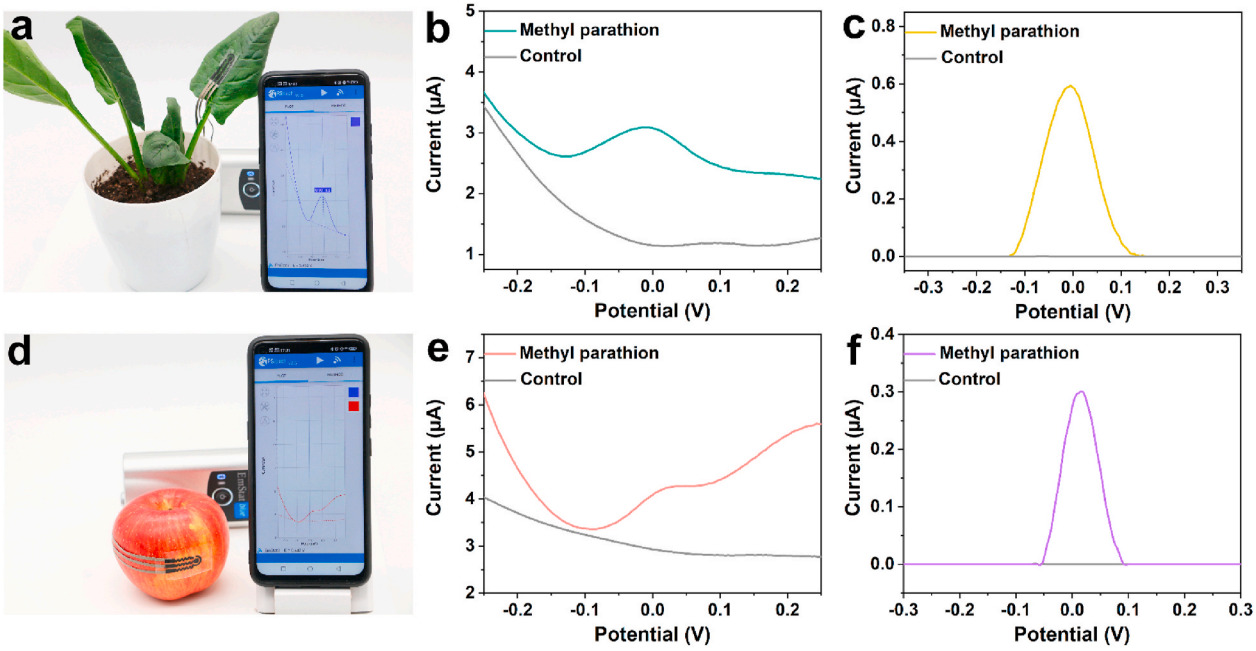

Fig. 6. In-situ OP analysis on the surfaces of different agricultural products. (a, d) Digital photos of the detection on (a) spinach and (d) apple contaminated surfaces. (b, e) SWV curves of samples contaminated with methyl parathion (100 μM) and control samples without methyl parathion. (c, f) The corresponding baseline-corrected SWV curves.

CRediT authorship contribution statement

Fengnian Zhao: prepared the materials and did electrochemical measurement. did the material characterization, prepared the manuscript. All authors commented on the manuscript. **Jianwei He:** did the material characterization. All authors commented on the manuscript. **Xunjia Li:** did the material characterization. All authors commented on the manuscript. **Yunpeng Bai:** Y.: supervised this project and designed the experiments. prepared the manuscript. All authors commented on the manuscript, supervised this project and designed the experiments. prepared the manuscript. All authors commented on the manuscript, prepared the manuscript. All authors commented on the manuscript. **Jianfeng Ping:** supervised this project and designed the experiments. prepared the manuscript. All authors commented on the manuscript.

Declaration of competing interest

The authors declare that they have no known competing financial interests or personal relationships that could have appeared to influence the work reported in this paper.

Acknowledgements

The authors acknowledge the financial support of the National Science Fund for Excellent Young Scholars of China (Grant No. 31922063) and Fundamental Research Funds for the Central Universities.

Appendix A. Supplementary data

Supplementary data to this article can be found online at https://doi.org/10.1016/j.bios.2020.112636.

References

Ashley, B.K., Brown, M.S., Park, Y., Kuan, S., Koh, A., 2019. Biosens. Bioelectron. 132, 343–351.
Chen, Y., Liu, H., Tian, Y., Du, Y., Ma, Y., Zeng, S., Gu, C., Jiang, T., Zhou, J., 2020. ACS Appl. Mater. Interfaces 12 (12), 14386–14399.
Chung, S.W., 2018. J. Sci. Food Agric. 98 (8), 2857–2870.
Chyan, Y., Ye, R., Li, Y., Singh, S.P., Arnusch, C.J., Tour, J.M., 2018. ACS Nano 12 (3), 2176–2183.
Cui, H.F., Wu, W.W., Li, M.M., Song, X., Lv, Y., Zhang, T.T., 2018. Biosens. Bioelectron. 99, 223–229.
Diego, A.-R., Teresa, G.-D., Isabel, D.-M., 2010. Food Chem. 122 (4), 1320–1326.
Giraldo, J.P., Wu, H., Newkirk, G.M., Kruss, S., 2019. Nat. Nanotechnol. 14 (6), 541–553.
Guinovart, T., Valdés-Ramírez, G., Windmiller, J.R., Andrade, F.J., Wang, J., 2014. Electroanalysis 26 (6), 1345–1353.
Guo, X., Zhou, H., Fan, T., Zhang, D., 2015. Sensor. Actuator. B Chem. 220, 33–39.
Hofmann, T., Lowry, G.V., Ghoshal, S., Tufenkji, N., Brambilla, D., Dutcher, J.R., Gilbertson, L.M., Giraldo, J.P., Kinsella, J.M., Landry, M.P., Lovell, W., Naccache, R., Paret, M., Pedersen, J.A., Unrine, J.M., White, J.C., Wilkinson, K.J., 2020. Nat. Food 1 (7), 416–425.
Imani, S., Bandodkar, A.J., Mohan, A.M., Kumar, R., Yu, S., Wang, J., Mercier, P.P., 2016. Nat. Commun. 7, 11650.
Karyakin, A.A., Karyakina, E.E., Gorton, L., 1996. Anal. Chem. 68, 4335–4341.
Kim, J., Campbell, A.S., de Avila, B.E.-F., Wang, J., 2019. Nat. Biotechnol. 37 (4), 389–406.
Lamberti, A., Clerici, F., Fontana, M., Scaltrito, L., 2016. Adv. Energy Mater. 6 (10), 1600050.
Lan, L., Le, X., Dong, H., Xie, J., Ying, Y., Ping, J., 2020. Biosens. Bioelectron. 165, 112360.
Lee, K., Park, J., Lee, M.S., Kim, J., Hyun, B.G., Kang, D.J., Na, K., Lee, C.Y., Bien, F., Park, J.U., 2014. Nano Lett. 14 (5), 2647–2654.
Li, Z., Paul, R., Ba Tis, T., Saville, A.C., Hansel, J.C., Yu, T., Ristaino, J.B., Wei, Q., 2019. Native Plants 5 (8), 856–866.
Lin, H., Zhou, H., Xu, L., Zhu, H., Huang, H., 2016. Biotechnol. Bioeng. 143, 42–49.
Lin, J., Peng, Z., Liu, Y., Ruiz-Zepeda, F., Ye, R., Samuel, E.L., Yacaman, M.J., Yakobson, B.I., Tour, J.M., 2014. Nat. Commun. 5, 5714.
Luo, X.J., Kong, X.D., Zhao, J., Chen, Q., Zhou, J., Xu, J.H., 2014. Biotechnol. Bioeng. 111 (10), 1920–1930.
Ma, Y., Yue, Y., Zhang, H., Cheng, F., Zhao, W., Rao, J., Luo, S., Wang, J., Jiang, X., Liu, Z., Liu, N., Gao, Y., 2018. ACS Nano 12 (4), 3209–3216.
Mishra, R.K., Hubble, L.J., Martin, A., Kumar, R., Barfidokht, A., Kim, J., Musameh, M. M., Kyratzis, I.L., Wang, J., 2017. ACS Sens. 2 (4), 553–561.
Nassar, J.M., Khan, S.M., Villalva, D.R., Nour, M.M., Almuslem, A.S., Hussain, M.M., 2018. npj Flex. Electron. 2 (1), 24.
Nguyen Thi, H., Nguyen, D.H., Vu, M.T., Tran, H.N., Pham Tran, L.P., Nguyen-Thi, N.-T., Le, N.T.T., Le Minh Tri, N., 2020. Mater. Res. Express 7 (3), 035019.
Nyein, H.Y., Gao, W., Shahpar, Z., Emaminejad, S., Challa, S., Chen, K., Fahad, H.M., Tai, L.C., Ota, H., Davis, R.W., Javey, A., 2016. ACS Nano 10 (7), 7216–7224.
Patel, N.G., Erlenkötter, A., Cammann, K., Chemnitius, G.-C., 2000. Sensor. Actuator. B Chem. 67, 134–141.
Paul, R., Saville, A.C., Hansel, J.C., Ye, Y., Ball, C., Williams, A., Chang, X., Chen, G., Gu, Z., Ristaino, J.B., Wei, Q., 2019. ACS Nano 13 (6), 6540–6549.
Sitjar, J., Liao, J.D., Lee, H., Pan, L.P., Liu, B.H., Fu, W.E., Chen, G.D., 2019. Nanomaterials 9 (12), 1750.
Tang, W., Yan, T., Ping, J., Wu, J., Ying, Y., 2017. Adv. Mater. Technol. 2 (7), 1700021.

Tang, W., Yan, T., Wang, F., Yang, J., Wu, J., Wang, J., Yue, T., Li, Z., 2019. Carbon 147, 295–302.
Xuan, X., Kim, J.Y., Hui, X., Das, P.S., Yoon, H.S., Park, J.Y., 2018. Biosens. Bioelectron. 120, 160–167.
Ye, H.X., Guo, Z.Z., Peng, M., Cai, C.Y., Chen, Y., Cao, Y.P., Zhang, W.Y., 2016. Electroanalysis 28 (7), 1591–1596.
Ye, R., James, D.K., Tour, J.M., 2019. Adv. Mater. 31 (1), e1803621.
You, Z., Qiu, Q., Chen, H., Feng, Y., Wang, X., Wang, Y., Ying, Y., 2019. Biosens. Bioelectron. 150, 111896.
Zhang, C., Ping, J., Ying, Y., 2020. Sci. Total Environ. 714, 136687.
Zhao, F., Wu, J., Ying, Y., She, Y., Wang, J., Ping, J., 2018a. TrAC Trends Anal. Chem. (Reference Ed.) 106, 62–83.
Zhao, F., Yao, Y., Jiang, C., Shao, Y., Barcelo, D., Ying, Y., Ping, J., 2019. J. Hazard Mater. 384, 121358.
Zhao, F., Yao, Y., Li, X., Lan, L., Jiang, C., Ping, J., 2018b. Anal. Chem. 90, 11658–11664.
Zhao, L., Lu, L., Wang, A., Zhang, H., Huang, M., Wu, H., Xing, B., Wang, Z., Ji, R., 2020. J. Agric. Food Chem. 68 (7), 1935–1947.